Acta. Chim. Asiana., 2026, 9(2), 910-919
e-ISSN/p-ISSN 2550-0503/2550-049x
Available online at: www.aca.unram.ac.id

RESEARCH PAPER

Coating Silicon Carbide Semiconductor with Soft Cations for Electrical Transfer in Energy-Saving Batteries: A Quantum DFT Study

Fatemeh Mollaamin*

Department of Biomedical Engineering, Faculty of Engineering and Architecture, Kastamonu University, Kastamonu, Turkey.

*e-mail: fmollaamin@kastamonu.edu.tr

DOI: https://doi.org/10.29303/aca.v9i2.309

Article info:

Received: 02/06/2026

Revised: 23/08/2026

Accepted: 05/11/2026

Available online: 05/11/2026

ABSTRACT: 2D silicon carbide (SiC) has been developed and tested as an anode material for batteries utilizing lithium (Li), sodium (Na), potassium (K), beryllium (Be), magnesium (Mg), boron (B), aluminum (Al), and gallium (Ga) ions. This is due to its ability to form nanoclusters such as SiCLi, SiCNa, SiCK, SiCBe, SiCMg, SiCB, SiCAl, and SiCGa. A comprehensive study was conducted to explore the energy-saving potential of these SiCLi, SiCNa, SiCK, SiCBe, SiCMg, SiCB, SiCAl, and SiCGa complexes. This study utilized computer methods to analyze charge density differences (CDD), total density of states (TDOS), and molecular electrostatic potential (ESP) for these hybrid nanoclusters. The addition of lithium, sodium, beryllium, and magnesium can increase the negative charge on carbon atoms, serving as electron acceptors in these nanoclusters. Increasing the presence of silicon and carbon in these nanoclusters can enhance battery capacity during energy storage and improve performance at higher rates by enhancing electrical conductivity. Additionally, using SiC as an anode could potentially extend battery lifespan by preventing electrode breakdown and increasing capacity due to stronger surface effects.

Keywords: Novel hybrid-ion batteries; silicon carbide; Groups 1,2,13 Metals; DFT

1 Introduction

The necessity for improved high-performance anodes in lithium-ion batteries has been emphasized. Researchers have explored the use of a nanomaterial, such as silicon carbide, which serves as a wide bandgap semiconductor with robust mechanical properties, as a potential anode. However, a significant challenge has been the substantial volume changes that occur during the charge and discharge cycles of silicon-based nanostructures utilized as anodes in high-energy batteries. This problem is considered the primary obstacle hindering the commercial application of these materials [1–4].

Alongside the low diffusion barrier, moderate open circuit voltage, and good electronic conductivity during sodiation, researchers have suggested that graphitic SiC could be a promising material for use as an anode in sodium-ion batteries. Furthermore, they found that enhancing the amount of covalent bonding in Na-C bonds can improve the ability of sodium ions to intercalate into carbon-based multilayer materials. This enhancement can be accomplished by doping with atoms such as Li, Be, B, Al, Si, or P, which have lower electronegativity compared to carbon atoms [5–9].

Researchers studied the structure of a single layer of silicon carbide (SiC) to determine its ability to store sodium and potassium ions. They utilized a method known as DFT for analysis. The findings revealed that SiC exhibits negative adsorption energies when potassium or sodium atoms bond to its surface, indicating an energetically favorable process. The single-layer SiC has the capacity to retain a high number of sodium or potassium ions on both sides of its surface. Additionally, the introduction of sodium or potassium causes the semiconducting SiC layer to transition into a metallic state with excellent electrical conductivity. These results suggest that the SiC monolayer could serve as a promising material for application in sodium-ion and potassium-ion batteries [10].

Researchers are investigating silicon carbide and III-nitride nanosheets as potential alternatives to lithium and sodium ion batteries for use in magnesium ion batteries (MIBs). Through calculations based on density functional theory, they discovered that MIBs utilizing these materials exhibit higher internal energy changes and cell voltages compared to the carbon-based nanomaterials previously discussed in literature [11].

Acta. Chim. Asiana., 2026, 9(2), 910-919
e-ISSN/p-ISSN 2550-0503/2550-049x
Available online at: www.aca.unram.ac.id

RESEARCH PAPER

Since silicon is more polarizable than a carbon atom, it is believed that Si-C/Si nanosurfaces may bond more strongly with other materials compared to pure carbon nanostructures [12–14]. Previous studies on energy-saving devices utilizing hydrogen adsorption were conducted using DFT calculations involving semiconductor-based nano-carbides such as Si/Ge/Sn/Pb [15], Mg-Al nanoalloys [16], and Al/C/Si-doped BN nanocomposites [17]. Nanomaterials with unique structures are extremely valuable in fields such as electrocatalysis, fuel cells, and energy conservation [18].

Recently, researchers have been investigating the electrochemical reactions and challenges associated with using silicon-based anodes in alkali metal-ion batteries. They have explored various methods, including designing the structure of silicon, modifying the surface of silicon-based materials, and creating silicon-based composites to enhance battery performance. As a result, it is now possible to discuss the future challenges and potential benefits of developing silicon-based anode materials for these types of batteries [19,20].

$$\hat{H}_s = -\sum_i^M \frac{1}{2}\overline{\nabla}_i^2 + \sum_i^M v_s(\vec{r}_i) = \sum_i^M \hat{h}_s \quad (1)$$

$$\hat{h}_s = -\frac{1}{2}\overline{\nabla}_i^2 + v_s(\vec{r}_i) \quad (2)$$

Equation (3) expresses all physically valid electronic densities for the system of non-interacting electrons using the single particle orbitals ψ_i.

$$\rho(\vec{r}) = \sum_i^M |\psi_i(\vec{r})|^2 \quad (3)$$

Finally, the total energy can be calculated using the KS method based on equation (4):

$$E[\rho] = \sum_i^M n_i \langle \psi_i \left| -\frac{1}{2}\overline{\nabla}^2 + v_{ext}(\vec{r}) + \frac{1}{2}\int \frac{\rho(\vec{r}')}{|\vec{r}-\vec{r}'|}\,d\vec{r}' \right| \psi_i \rangle + E_{xc}[\rho] + \frac{1}{2}\sum_\beta^N \sum_{\alpha\neq\beta}^N \frac{Z_\alpha Z_\beta}{|\vec{R}_\alpha - \vec{R}_\beta|} \quad (4)$$

Therefore, the exact exchange energy functional is described using Kohn-Sham orbitals instead of the density, which is referred to as the indirect density functional. This study utilized the hybrid functional with a three-parameter basis set called B3LYP (Becke, Lee, Yang, Parr) within the framework of DFT for theoretical calculations. The widely used B3LYP (Becke, three-parameter, Lee-Yang-Parr) and exchange-correlation functional are based on equation (5) [23–25]:

$$E_{XC}^{B3LYP} = (1-\alpha)E_X^{LSDA} + \alpha E_X^{HF} + b\Delta E_X^B + (1-c)E_C^{LSDA} + cE_C^{LYP} \quad (5)$$

Calculations that consider spin polarization were carried out using density functional theory (DFT) [26]. The exchange correlation potentials were handled with the Perdew–Burke–Ernzerhof (PBE) method, which is part of the general gradient approximation (GGA) [27,28]. Figure 1 shows nanoclusters made from Group 1, 2, and 13 metals, specifically SiCLi, SiCNa, SiCK, SiCBe, SiCMg, SiCB, SiCAl, and SiCGa.

In another study, Dong and his team used titanium silicon carbide (Ti_3SiC_2, TSC) to create a silicon-based anode composite (Si/TSC) to enhance the performance of lithium-ion batteries. They utilized TSC as a material to reinforce the structure and enhance conductivity for the silicon anode. After conducting a detailed analysis, they tested the samples to observe how their performance correlated with changes in chemical composition. This helped them assess the material's effectiveness for battery applications involving lithium, sodium, potassium, beryllium, magnesium, boron, aluminum, or gallium.

2. Theoretical Backgrounds, Materials and Methods

The applied Density Functional Theory (DFT) approach gained significant attention only after W. Kohn and L. J. Sham published their well-regarded set of equations, known as the Kohn-Sham (KS) equations [21,22].

Acta. Chim. Asiana., 2026, 9(2), 910-919
e-ISSN/p-ISSN 2550-0503/2550-049x
Available online at: www.aca.unram.ac.id

RESEARCH PAPER

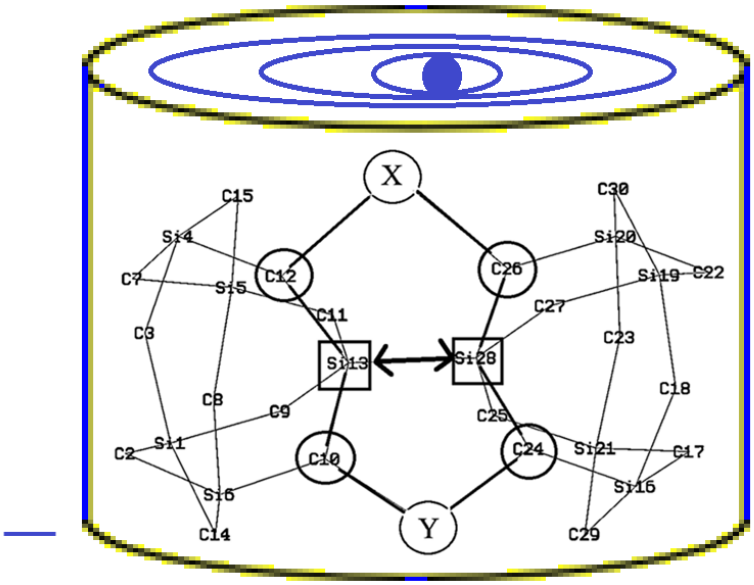


Figure1. Adding Li, Na, K, Be, Mg, B, Al or Ga to SiC nanocluster and formation of SiCLi, SiCNa, SiCK, SiCBe, SiCMg, SiCB, SiCAl, or SiCGa complexes towards energy storage in novel batteries. (X Y= LiLi, NaNa, KK, BeBe, Mg,Mg BB, AlAl, or GaGa).

The Bader charge parameter analysis [29] has been conducted for energy storage using hybrid clusters consisting of SiCLi, SiCNa, SiCK, SiCBe, SiCMg, SiCB, SiCAl, and SiCGa complexes (Figure 1). This analysis was performed using the Gaussian 16 revision C.01 computational software [30] and the GaussView 6.1 graphical program [31].

Using silicon carbide nanoclusters as the anode in batteries that run on lithium, sodium, beryllium, magnesium, boron, aluminum, or gallium offers several key benefits. These nanoclusters allow for multiple ways to store ions like lithium, sodium, beryllium, or magnesium within a stable silicon carbide structure. They also improve electrical conductivity because of the silicon and carbon in the material, and the nanocluster shape helps increase the surface area. In this study, silicon or carbon can be evenly spread out within the silicon carbide matrix, which prevents them from clumping together during repeated charge and discharge cycles. When lithium, sodium, beryllium, or magnesium ions are inserted into the material, some of the carbon bonds - like C-Li, C-Na, C-Be, or C-Mg - may break, causing slight expansion. This creates better spots for more ions to insert into the material later on, as shown in Figure 1.

3. Results and Discussion

3.1. Charge distribution analysis

The charge distribution of elements from C(2), C(3), C(7) through C(12), C(14), C(15), C(17), C(18), C(22) through C(27), C(29), and C(30) in the nanoclusters made of SiCLi, SiCNa, SiCK, SiCBe, SiCMg, SiCB, SiCAl, and SiCGa has been observed in Table 1.

Table 1. The atomic charge (Q/coulomb) for SiCLi, SiCNa, SiCK, SiCBe, SiCMg, SiCB, SiCAl, SiCGa nanoclusters.

SiCLi		SiCNa		SiCK		SiCBe	
Atom	Q	Atom	Q	Atom	Q	Atom	Q
C(2)	–0.42	C(2)	–0.42	C(2)	–0.43	C(2)	–0.43
C(3)	–0.34	C(3)	–0.37	C(3)	–0.34	C(3)	–0.36
C(7)	–0.38	C(7)	–0.40	C(7)	–0.39	C(7)	–0.39
C(12)	–0.92	C(12)	–0.82	C(12)	–0.90	C(12)	–0.89
C(14)	–0.37	C(14)	–0.37	C(14)	–0.36	C(14)	–0.36
C(15)	–0.38	C(15)	–0.38	C(15)	–0.41	C(15)	–0.34
C(17)	–0.41	C(17)	–0.42	C(17)	–0.43	C(17)	–0.41
C(18)	–0.35	C(18)	–0.37	C(18)	–0.38	C(18)	–0.34

SiCLi		SiCNa		SiCK		SiCBe	
C(27)	–0.51	C(27)	–0.47	C(27)	–0.46	C(27)	–0.49
C(29)	–0.40	C(29)	–0.39	C(29)	–0.42	C(29)	–0.37
C(30)	–0.37	C(30)	–0.39	C(30)	–0.37	C(30)	–0.34
Li(31)	0.75	Na(31)	0.68	K(31)	0.91	Be(31)	0.65
Li(32)	0.50	Na(32)	0.37	K(32)	0.90	Be(32)	0.67
SiCMg		SiCB		SiCAl		SiCGa	
Atom	Q	Atom	Q	Atom	Q	Atom	Q
C(2)	–0.43	C(2)	–0.42	C(2)	–0.42	C(2)	–0.42
C(3)	–0.34	C(3)	–0.34	C(3)	–0.33	C(3)	–0.33
C(7)	–0.39	C(7)	–0.38	C(7)	–0.39	C(7)	–0.39
C(8)	–0.34	C(8)	–0.36	C(8)	–0.34	C(8)	–0.34
C(9)	–0.35	C(9)	–0.38	C(9)	–0.34	C(9)	–0.35
C(10)	–1.07	C(10)	–0.76	C(10)	–1.23	C(10)	–1.14
C(11)	–0.37	C(11)	–0.36	C(11)	–0.33	C(11)	–0.34
C(12)	–1.10	C(12)	–0.81	C(12)	–1.08	C(12)	–1.01
C(14)	–0.38	C(14)	–0.33	C(14)	–0.35	C(14)	–0.34
C(15)	–0.38	C(15)	–0.34	C(15)	–0.35	C(15)	–0.35
C(17)	–0.42	C(17)	–0.43	C(17)	–0.43	C(17)	–0.43
C(18)	–0.34	C(18)	–0.36	C(18)	–0.35	C(18)	–0.34
C(22)	–0.39	C(22)	–0.38	C(22)	–0.38	C(22)	–0.38
C(23)	–0.35	C(23)	–0.35	C(23)	–0.33	C(23)	–0.33
C(24)	–1.05	C(24)	–0.77	C(24)	–1.20	C(24)	–1.10
C(25)	–0.32	C(25)	–0.35	C(25)	–0.33	C(25)	–0.34
C(26)	–1.06	C(26)	–0.76	C(26)	–1.07	C(26)	–1.00
C(27)	–0.48	C(27)	–0.45	C(27)	–0.41	C(27)	–0.42
C(29)	–0.42	C(29)	–0.30	C(29)	–0.34	C(29)	–0.33
C(30)	–0.37	C(30)	–0.34	C(30)	–0.36	C(30)	–0.35
Mg(31)	1.15	B(31)	0.40	Al(31)	0.93	Ga(31)	0.76
Mg(32)	1.09	B(32)	0.32	Al(32)	1.13	Ga(32)	0.92

The distribution of electric charge has been shown for Groups 1, 2, and 13 metals that are captured by the SiC nanostructure, leading to the formation of nanoclusters such as SiCLi, SiCNa, SiCK, SiCBe, SiCMg, SiCB, SiCAl, and SiCGa (Table 1). When Li, Na, K, Be, Mg, B, Al, or Ga atoms are attached, they help increase the negative charge on specific carbon atoms like C(2), C(3), C(7) through C(12), C(14), C(15), C(17), C(18), C(22) through C(27), C(29), and C(30), making them act as electron acceptors in these nanoclusters (Table 1) [32].

3.2. Total Density of States

In an isolated system, such as a single molecule, the energy levels are distinct and separate. Due to this, the concept of "density of states (DOS)" is not applicable in this scenario. Therefore, the "original total DOS (TDOS)" for such an isolated system can be represented as [33].

$$TDOS\,(E) = \sum_i \delta\,(E - \epsilon_i) \quad (6)$$

The normalized Gaussian function is defined as:

$$G(x) = \frac{1}{c\sqrt{2\pi}} e^{-\frac{x^2}{2c^2}} \text{ where } c = \frac{\text{FWHM}}{2\sqrt{2\ln x}} \quad (7)$$

FWHM (full width at half maximum)" is an adjustable setting in "Multiwfn" [34, 35]. In addition, the curve maps for "broadened partial DOS (PDOS)" and "overlap DOS (OPDOS)" are helpful for analyzing the composition of orbitals. The "PDOS function of fragment "*A*" is defined as:

$$PDOS_A\,(E) = \sum_i \Xi_{i,A}\, F\,(E - \epsilon_i) \quad (8)$$

Acta. Chim. Asiana., 2026, 9(2), 910-919
e-ISSN/p-ISSN 2550-0503/2550-049x
Available online at: www.aca.unram.ac.id

RESEARCH PAPER

where " $\Xi_{i,A}$ " represents the composition of fragment "*A*" in orbital "*i*". The 'OPDOS between fragment "*A*" and "*B*" is defined as:

$$OPDOS_{A,B}(E) = \sum_i X^i_{A,B} F(E - \epsilon_i) \quad (9)$$

The term " $X^i_{A,B}$ " represents the total cross term between fragments "*A*" and "*B*" in orbital "*i*". In terms of the energy storage capability of SiCLi, SiCNa, SiCK, SiCBe, SiCMg, SiCB, SiCAl, and SiCGa nanoclusters, the total density of states (TDOS) has been analyzed. This analysis reveals the presence of significant chemical interactions, typically located on the "convex side" as illustrated in Figures 2(a–h).

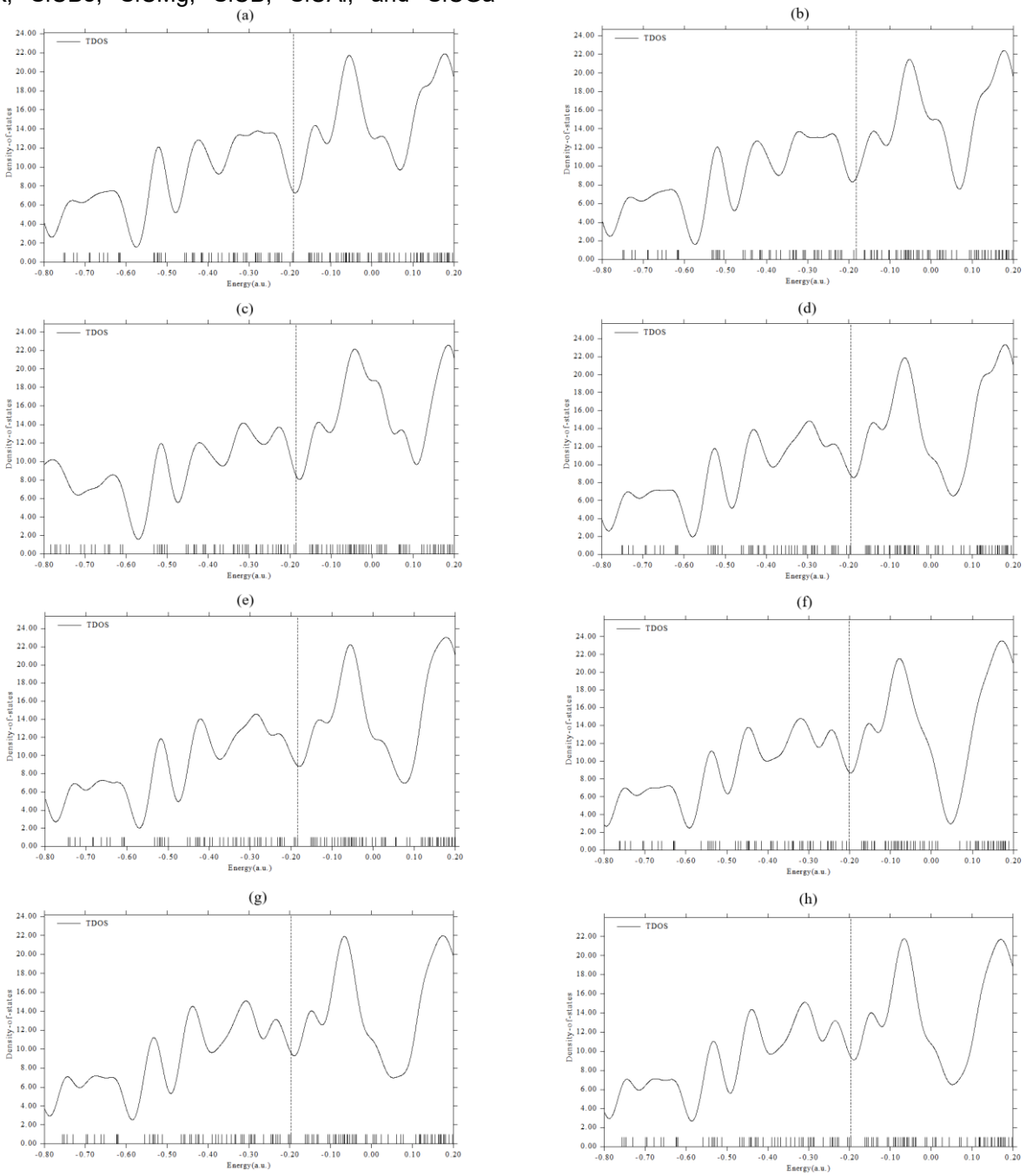


Figure 2. TDOS graphs of (a) SiCLi, (b) SiCNa, (c) SiCK, (d) SiCBe, (e) SiCMg, (f) SiCB, (g) SiCAl, (h) SiCGa nanoclusters.

Acta. Chim. Asiana., 2026, 9(2), 910-919
e-ISSN/p-ISSN 2550-0503/2550-049x
Available online at: www.aca.unram.ac.id

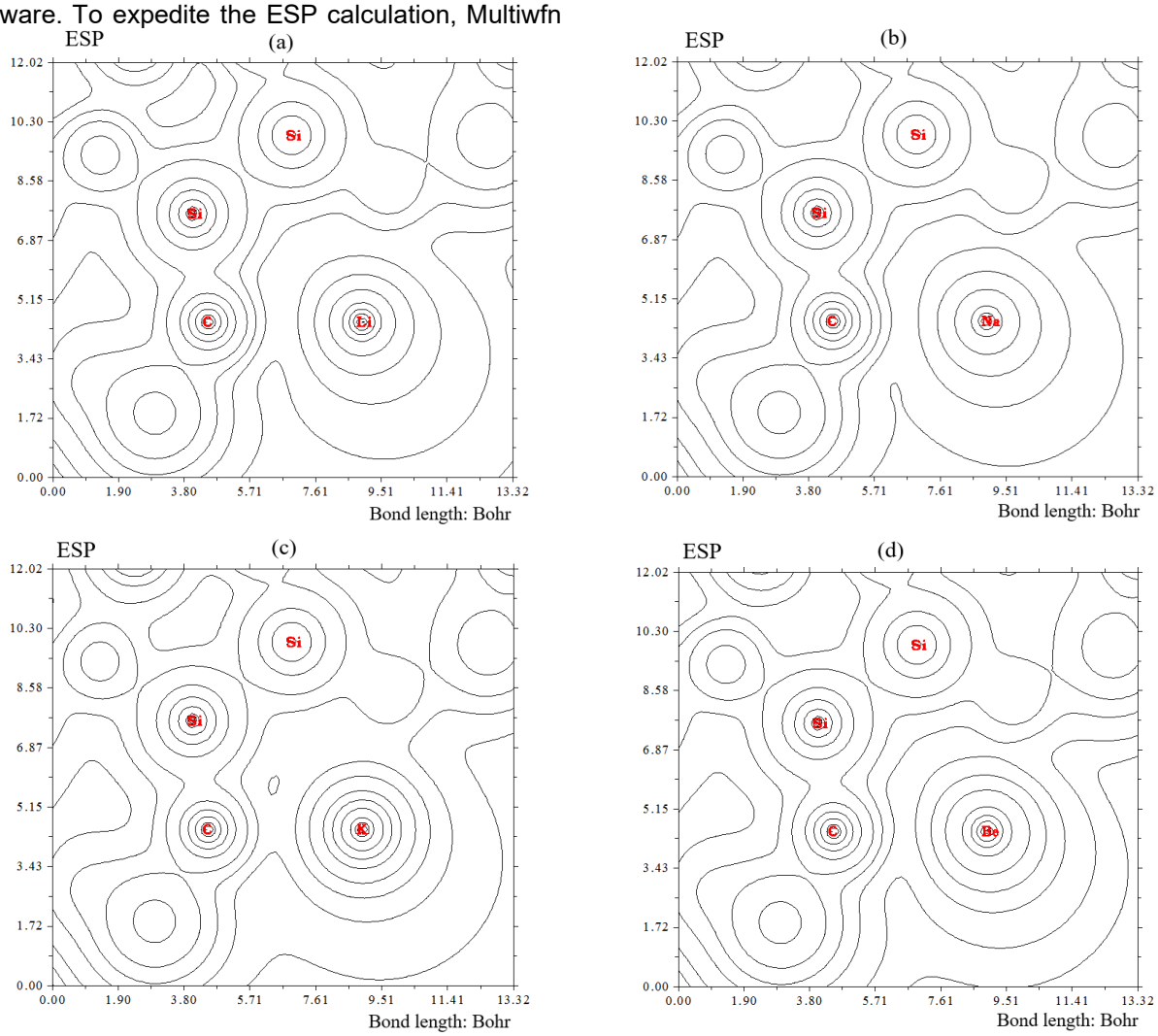
RESEARCH PAPER

3.3. Molecular electrostatic potential (ESP)

The molecular electrostatic potential (ESP) has long been used to identify potential nucleophilic and electrophilic attack sites. It is also useful in understanding hydrogen bonds, halogen bonds, molecular recognition, and interactions between aromatic molecules [36]. This function calculates the electrostatic interaction between a single point charge at a specific location and the molecule under study. A positive value indicates that the area is primarily influenced by nuclear charges, while a negative value suggests it is more affected by electronic charges.

$$V_{tot}(r) = V_{nuc}(r) + V_{ele}(r) = \sum_A \frac{Z_A}{|r-R_A|} - \int \frac{\rho(r')}{|r-r'|} dr' \quad (10)$$

Z_A refers to the nuclear charge. If you are using a pseudopotential, then Z_A represents the number of electrons that are explicitly shown. It is important to note that calculating the electrostatic potential (ESP) takes much longer than calculating other functions. In Multiwfn, ESP is calculated exactly using nuclear attractive integrals, rather than with approximate methods like multipole expansion or solving the numerical Poisson equation. Due to this, the ESP results from Multiwfn might appear different from those produced by other quantum chemistry software. To expedite the ESP calculation, Multiwfn skips some integrals that contribute minimally to the final result. The cutoff value for which integrals are skipped is set in "espprecutoff" in settings.ini. Increasing this value enhances the accuracy of the ESP but also increases the computational workload. In most scenarios, the ESP calculated with the default setting is sufficiently accurate. Atoms of Li, Na, K, Be, Mg, B, Al, or Ga are enclosed by a silicon carbide (SiC) nanostructure (Figure 3a–h) to create nanoclusters such as SiCLi, SiCNa, SiCK, SiCBe, SiCMg, SiCB, SiCAl, and SiCGa (Figure 3a–h).



Acta. Chim. Asiana., 2026, 9(2), 910-919
e-ISSN/p-ISSN 2550-0503/2550-049x
Available online at: www.aca.unram.ac.id

RESEARCH PAPER

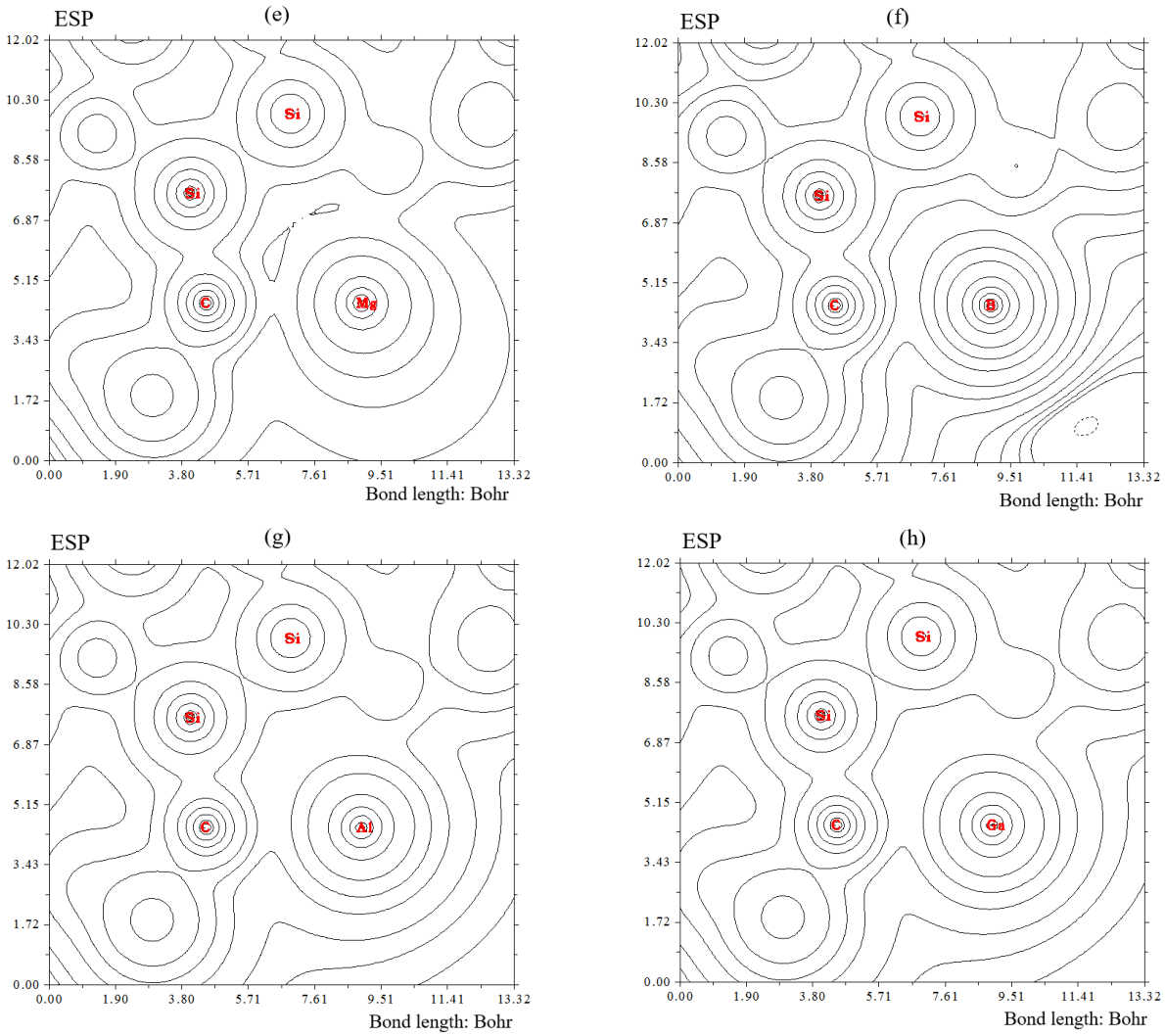


Figure 3. The shaded (left side) and counter (right side) maps of ESP graphs for (a) SiCLi, (b) SiCNa, (c) SiCK, (d) SiCBe, (e) SiCMg, (f) SiCB, (g) SiCAl, (h) SiCGa nanoclusters.

SiCLi (Figure 3a), SiCNa (Figure 3b), SiCK (Figure 3c), SiCBe (Figure 3d), SiCMg (Figure 3e), SiCB (Figure 3f), SiCAl (Figure 3g), and SiCGa (Figure 3h) have shown electron delocalization through an isosurface map. Labeled atoms include C(10), C(12), Si(13), C(24), C(26), Si(28), X(31)/X(32) (where X is Li, Na, K, Be, Mg, B, Al, or Ga). The counter map of ESP confirms that these SiCLi, SiCNa, SiCK, SiCBe, SiCMg, SiCB, SiCAl, and SiCGa nanoclusters may improve the efficiency of energy storage (Figure 3a–h and Table 2).

Table2. Cell capacity (C, mAh g^{-1}), dipole moment (D/debye), HOMO(eV), LUMO (eV), energy gap ($\Delta E = E_{LUMO} - E_{HOMO}$ /eV) and stability energy (E_s/kcal/mol) for SiCLi, SiCNa, SiCK, SiCBe, SiCMg, SiCB, SiCAl, SiCGa nanoclusters.

Heteroclusters	C	D	E_{HOMO}	E_{LUMO}	ΔE	$E_s \times 10^{-3}$
SiCLi	100.20	1.25	–5.20	–4.20	1.00	–509.21
SiCNa	94.53	1.18	–4.96	–4.43	0.52	–499.96
SiCK	453.1410	0.9438	–5.05	–4.13	0.9275	–534.83
SiCBe	198.86	1.09	–5.30	–4.33	0.97	–518.21
SiCMg	188.18	0.29	–5.06	–4.12	0.89	–500.80
SiCB	2605.62	0.61	–5.49	–4.61	0.88	–530.75
SiCAl	1709.64	1.26	–5.35	–4.40	0.95	–502.24

RESEARCH PAPER

Heteroclusters	C	D	E_{HOMO}	E_{LUMO}	ΔE	$E_s \times 10^{-3}$
SiCGa	895.66	1.11	–5.36	–4.41	0.95	–502.32

Moreover, the intermolecular orbital overlap integral plays a crucial role in discussions regarding intermolecular charge transfer. This integral is utilized to calculate the HOMO–HOMO and LUMO–LUMO overlaps between Group 1, 2, and 13 metals and silicon carbide (Table 2).

4. Conclusions

Metals from Groups 1, 2, and 13 were examined for their ability to interact with silicon carbide and create nanoclusters such as SiCLi, SiCNa, SiCK, SiCBe, SiCMg, SiCB, SiCAl, and SiCGa through computational methods. The research revealed significant changes in charge density, indicating a noticeable transfer of charge within these compounds. Silicon carbide, known for its semiconductor properties, is often combined with carbon to enhance both ionic and electronic conductivity. The addition of elements like lithium, sodium, potassium, beryllium, magnesium, boron, aluminum, or gallium to battery cells is recognized for its ability to increase energy efficiency.

Acknowledgement: The author is grateful to Kastamonu University for completing this paper and its research.

References

1. Adrian Nur, Anatta W. Budiman, Arif Jumari, Nazriati Nazriati, Fauziatul Fajaroh, Electrosynthesis of Ni-Co/Hydroxyapatite as a Catalyst for Hydrogen Generation via the Hydrolysis of Aqueous Sodium Borohydride ($NaBH_4$) Solutions. Chem. Chem. Technol. 15(3), 389–394 (2021). https://doi.org/10.23939/chcht15.03.389
2. Ruslana Guminilovych, Pavlo Shapoval, Iosyp Yatchyshyn, Stepan Shapoval, Synthesis, Structure and Electrophysical Properties of Fluoride-Conducting Phases Ba1-XLaXSnF4+X. Chem. Chem. Technol. 18(3), 313-320 (2024). https://doi.org/10.23939/chcht18.03.313
3. Leonid Kovalenko, Ivan Lisovskyi, Volodymyr Khomenko, Dmytro Patlun, Oleksandr Potapenko, Anatolii Belous, Development of Membranes Based on Polyvinylidene Fluoride for Lithium Batteries. Chem. Chem. Technol. 19(2), 270–276 (2025). https://doi.org/10.23939/chcht19.02.270
4. Aseel Hadi, Saba R. Salman, Najah M. L. Al Maimuri, Ahmed Hashim, Farhan Lafta Rashid, Ali S. Hasan, Synthesis and Tailoring the Optimization and Dielectric Properties of PMMA/PEG/Barium Titanate Hybrid Nanostructures for Energy Storage and Electronics Applications. Chem. Chem. Technol. 19(2), 277–285 (2025). https://doi.org/10.23939/chcht19.02.277
5. G. Shao, D. A. H. Hanaor, J. Wang, D. Kober, S. Li, X. Wang, X. Shen, M. F. Bekheet, A. Gurlo, *ACS Appl. Mater. Interfaces* 2020, *12*, 46045. https://doi.org/10.1021/acsami.0c12376
6. Mollaamin, F. Anchoring of 2D layered materials of $Ge_5Si_5O_{20}$ for (Li/Na/K)-(Rb/Cs) batteries towards Eco-friendly energy storage. *BMC Chemistry* 19, 233 (2025). https://doi.org/10.1186/s13065-025-01593-0
7. M. Wilamowska-Zawlocka, P. Puczkarski, Z. Grabowska, J. Kaspar, M. Graczyk-Zajac, R. Riedel, G. D. Sorarù, *RSC Adv.* 2016, *6*, 104597. https://doi.org/10.1039/C6RA24539K
8. Nataliia Zabiiaka, Nadiia Kanunnikova, Oleksandr Haiduchok, Chemical hydrogen production from aluminum alloy ak7 using naf and nacl activators for emergency power supply systems. Chem. Chem. Technol. 19(4), 601–611 (2025). https://doi.org/10.23939/chcht19.04.601
9. Qin Liu, Chengbin Fu, Bo Xiao, Yanchun Li, Jianbo Cheng, Zhenbo Liu, Xin Yang, Xiufeng Xu, Hongtao Cui, Qingzhong Li, Graphitic SiC: A potential anode material for Na-ion battery with extremely high storage capacity. International Journal of Quantum Chemistry. 121(10), e26608 (2021). https://doi.org/10.1002/qua.26608
10. Qiong Peng, Javed Rehman, Mohib Ullah, Ammar M. Tighezza, Muhammad Bilal Hanif, M.F. Shibl, Jiayu Dai, Anchoring of K and Na on the surface of a novel SiC monolayer: First-principles predictions. Journal of Energy Storage. 104, 114435 (2024). https://doi.org/10.1016/j.est.2024.114435
11. Ghaith Ahmed, Arshad Fadhil Kadhim, Najah M. L. Al Maimuri, Hamed Ibrahim, Ahmed Hashim, Mohammed H. Abbas, Fabrication and Tailoring the Morphological and Electrical Features of Silicon Nitride-Silicon Dioxide/Polymethyl Methacrylate Hybrid Nanocomposites for Nanoelectronics Fields. Chem. Chem. Technol. 19(3), 495–502 (2025). https://doi.org/10.23939/chcht19.03.495
12. Abhijit Jadhav, Govindaraj Mohanraj, Suseeladevi Mayadevi, Ashok Gokarn,

Adsorption of Heavy Metal on Active Carbon Derived from Coconut Leaves Agro-Waste. Chem. Chem. Technol. 14(4), 553–562 (2020). https://doi.org/10.23939/chcht14.04.553

13. Hayam Osman Taha, Atef M. El Mahdy, Fatma El Sayed El Shemy, Mohammed Mohammed Hassan, Hydrogen storage in SiC, GeC, and SnC nanocones functionalized with nickel, Density Functional Theory—Study. International Journal of uantum Chemistry. 2023, 123 (3), e27023.https://doi.org/10.1002/qua.27023.
14. Wei, T., Zhou, Y., Sun, C. *et al.* An intermittent lithium deposition model based on CuMn-bimetallic MOF derivatives for composite lithium anode with ultrahigh areal capacity and current densities. *Nano Res.* (2023). https://doi.org/10.1007/s12274-023-6187-8
15. Mollaamin, F., Monajjemi, M. Nanomaterials for Sustainable Energy in Hydrogen-Fuel Cell: Functionalization and Characterization of Carbon Nano-Semiconductors with Silicon, Germanium, Tin or Lead through Density Functional Theory Study. *Russ. J. Phys. Chem. B* 18, 607–623 (2024). https://doi.org/10.1134/S1990793124020271
16. Mollaamin, F., Shahriari, S. & Monajjemi, M. Influence of Transition Metals for Emergence of Energy Storage in Fuel Cells through Hydrogen Adsorption on the MgAl Surface. *Russ. J. Phys. Chem. B* 18, 398–418 (2024). https://doi.org/10.1134/S199079312402026X
17. Mollaamin, F., Monajjemi, M. Electric and Magnetic Evaluation of Aluminum–Magnesium Nanoalloy Decorated with Germanium Through Heterocyclic Carbenes Adsorption: A Density Functional Theory Study. *Russ. J. Phys. Chem. B* **17**, 658–672 (2023). https://doi.org/10.1134/S1990793123030223
18. Mollaamin, F.; Monajjemi, M. Adsorption ability of Ga_5N_{10} nanomaterial for removing metal ions contamination from drinking water by DFT. Int. J. Quantum Chem. 124(2), e27348 (2024). https://doi.org/10.1002/qua.27348
19. Foysal Kabir Tareq, Souman Rudra, Enhancing the performance of silicon-based anode materials for alkali metal (Li, Na, K) ion battery: A review on advanced strategies. Materials Today Communication, Volume 39, June 2024, 108653. https://doi.org/10.1016/j.mtcomm.2024.108653
20. Z. Dong, H. Gu, W. Du, Z. Feng, C. Zhang, Y. Jiang, T. Zhu, G. Chen, J. Chen, Y. Liu, Si/Ti3SiC2 composite anode with enhanced elastic modulus and high electronic conductivity for lithium-ion batteries. J. Power Sources, 431 (2019), 55-62. https://doi.org/10.1016/j.jpowsour.2019.05.043
21. Kohn, W.; Sham, L. J. Self-Consistent Equations Including Exchange and Correlation Effects.Phys. Rev., 1965, 140, A1133- A1138.
22. Hohenberg, P.; Kohn, W. Inhomogeneous Electron Gas. Phys. Rev. B, 1964, 136, B864-B871.
23. Becke AD (1993) Density-functional thermochemistry. III. The role of exact exchange. J Chem Phys 98:5648–5652.
24. Lee C, Yang W, Parr RG (1988) Development of the Colle–Salvetti correlation-energy formula into a functional of the electron density. Phys Rev B 37:785–789.
25. S. H. Vosko; L. Wilk; M. Nusair (1980). "Accurate spin-dependent electron liquid correlation energies for local spin density calculations: a critical analysis". Can. J. Phys. 58 (8): 1200–1211. Bibcode:1980CaJPh..58.1200V. doi:10.1139/p80-159.
26. Stefan Grimme, Jens Antony, Stephan Ehrlich, Helge Krieg, A consistent and accurate ab initio parametrization of density functional dispersion correction (DFT-D) for the 94 elements H-Pu. J Chem Phys. 2010, 132(15):154104. doi: 10.1063/1.3382344.
27. J.P. Perdew, K. Burke & M. Ernzerhof, Generalized Gradient Approximation Made Simple. Phys. Rev. Lett. 77, 3865 (1996). https://doi.org/10.1103/PhysRevLett.77.3865
28. Mollaamin, F. Investigating the Treatment of Transition Metals for Ameliorating the Ability of Boron Nitride for Gas Sensing & Removing: A Molecular Characterization by DFT Framework. *Prot Met Phys Chem Surf* **60**, 1050–1063 (2024). https://doi.org/10.1134/S2070205124702502
29. G Henkelman, A Arnaldsson, and H Jónsson, “A fast and robust algorithm for Bader decomposition of charge density,” Computational Materials Science 36(3), 354-360 (2006). https://doi.org/10.1016/j.commatsci.2005.04.010
30. Frisch, M. J.; Trucks, G. W.; Schlegel, H. B.; Scuseria, G. E.; Robb, M. A.; et al. Gaussian 16, Revision C.01, Gaussian, Inc., Wallingford CT, 2016.

31. GaussView, Version 6.06.16, Dennington, Roy; Keith, Todd A.; Millam, John M. Semichem Inc., Shawnee Mission, KS, 2016.

32. Zihan Xu, Chenglong Qin, Yushu Yu, Gang Jiang, Liang Zhao, First-principles study of adsorption, dissociation, and diffusion of hydrogen on α-U (110) surface. AIP Advances 14, 055114 (2024). https://doi.org/10.1063/5.0208082

33. Mollaamin, F. Alkali Metals Doped on Tin-Silicon and Germanium-Silicon Oxides for Energy Storage in Hybrid Biofuel Cells: A First-Principles Study. *Russ. J. Phys. Chem. B* **19**, 722–736 (2025). https://doi.org/10.1134/S1990793125700393

34. T. Lu & F. Chen, J. Comput. Chem. 33, 580–592 (2012). https://doi.org/10.1002/jcc.22885

35. T. Lu, J. Chem. Phys. 161, 082503 (2024). https://doi.org/10.1063/5.0216272

36. Jane S. Murray, Peter Politzer, The electrostatic potential: an overview. WIREs Comput. Mol. Sci., 1(2), 153-163 (2011). https://doi.org/10.1002/wcms.19.